NOVEL ANALYTICAL SOLUTIONS FOR TIME-FRACTIONAL THIN-FILM FERROELECTRIC MATERIAL MODEL

by

Ruyuan DU[a], Huajun ZENG[b], and Can LI[c*]

[a] Zhejiang Chang Xin Optotech Co., Ltd., Hangzhou, China
[b] School of Statistics and Mathematics, Zhejiang Gongshang University, Hangzhou, China
[c] School of Mathematics and Statistics, Hunan University of Technology and Business, Changsha, China

Original scientific paper
https://doi.org/10.2298/TSCI2602887D

Thin-film ferroelectric materials have been identified as having significant technological promise in microelectronics, optoelectronics, and sensor applications owing to their distinctive physical properties. The equation for thin-film ferroelectric materials with time-fractional derivatives offers enhanced precision in modeling the physical properties of such systems. The present study proposes a modified extended tanh-function approach to derive novel analytical solutions for the time-fractional thin-film ferroelectric material model. This method has been successfully implemented to derive various exact solutions to the model and plot their 3-D graphs. The findings of this study offer novel theoretical underpinnings for both the theoretical research and practical applications of thin-film ferroelectric materials.

Keywords: *time-fractional thin-film ferroelectric material model, novel analytical solution, modified extended tanh-function approach*

Introduction

Thin-film ferroelectric materials (TFFEM) [1] are a category of film materials that exhibit ferroelectric properties. These materials demonstrate a thickness of less than 1 μm and exhibit exceptional integrability across various device architectures. These elements are widely acknowledged as foundational components within the fields of microelectronics, optoelectronics, and emerging energy technologies [2-5]. Ferroelectric materials have attracted considerable research attention in the domain of thin-film fabrication due to their distinct material specificity. In contrast to conventional materials, TFFEM exhibit distinctive characteristics such as ultrahigh dielectric permittivity, enhanced capacitive density, superior polarization magnitude, along with remarkable environmental stability and field-tunable performance [6, 7]. Of particular significance is their ferroelectric property, which enables the material to undergo a reversible polarization process when exposed to an external electric field, while retaining a stable polarization state upon the removal of the field [8-10].

The polarization response characteristics of TFFEM are conducive to their implementation in the fabrication of multifunctional sensing devices, including photoelectric sensors [11, 12], pressure transducers [13], and analogous devices. The conversion of external mechanical stress or pressure into electrical signals by TFFEM is facilitated by the piezoelec-

* Corresponding author, e-mail: 1946@hutb.edu.cn

tric effect [14, 15], thereby enabling the detection of environmental changes [16]. Consequently, sensors fabricated from these materials exhibit critical advantages, including fast response speed, high sensitivity, and low power consumption, finding significant applications in medical [17], automotive [18], and smart device fields [19]. In the domain of microelectronics, TFFEM find extensive application in non-volatile memory devices, *e.g.*, FeRAM, owing to their capacity to retain information in the absence of a power supply [20, 21]. The FeRAM exhibits superior read/write speeds, reduced power consumption, and enhanced endurance when compared to conventional Flash memory or dynamic random-access memory [22]. In the domain of integrated circuits, TFFEM find application in low-voltage, miniaturized electronic components. Their high dielectric permittivity and robust polarization properties make them ideal for fabricating high-efficiency capacitors [23], electric-field-tunable devices [24, 25], and switching elements [26]. The non-linear electrical characteristics of these films have enabled the development of advanced electronic switches and logic circuits, which have found extensive applications in computer memory systems [27], wireless communications [28], intelligent sensing systems [29], and miniaturized devices [30].

In the domain of mathematical physics, the non-linear properties of TFFEM have garnered considerable attention. The implementation of mathematical models to describe these materials enables researchers to enhance the precise understanding and quantitative analysis of such complex physical phenomena. Furthermore, the solutions to these models can function as a foundational framework for the design and optimization of materials. Hubert *et al.* [31] derived the governing equations for TFFEM, which model the polarization propagation within these films and describe their electrical properties and behaviors under varying electric fields and temperature conditions. The study also revealed periodic soliton solutions of this system. Since that time, a considerable number of researchers have employed a variety of methods to obtain precise analytical solutions to this model. For instance, Zaharan *et al.* [32] employed MSEM and RBSODM methods to derive two types of solutions for the TFFEM equation. Furthermore, Bekir and Zahran [33] and Bekir *et al.* [34] employed the Painleve method and the (G'/G)-expansion method to explore distinct optical soliton solutions for this model. Chu *et al.* [35] applied a sinh-Gordon-based analytical framework to generate three classes of exact solutions: kink solitons, bright solitons, and periodic waves. Souleymanou *et al.* [36] derived soliton solutions through the employment of the modified extended tanh method. Chen and Li [37] derived traveling wave solutions by employing the complete discrimination system method. As previously referenced, Sadaf *et al.* [38] implemented the (G'/G,1/G)-expansion method and the generalized Kudryashov method to obtain a variety of solutions.

In recent years, there has been an intensification of academic research on PDE. Concurrently, scholarly focus has undergone a progressive shift from integer PDE to their fractional-order counterparts. Fractional PDE, defined by derivatives of fractional order, have been demonstrated to exhibit superior capacity in modeling non-linear phenomena [39, 40]. Consequently, to further explore the non-linear dynamics of ferroelectric particles, researchers have conducted studies on fractional-order formulations of the TFFEM equation. For instance, Faridi *et al.* [41] employed the (G'/G^2)-expansion technique and a novel extended direct algebraic approach to obtain various solitary wave solutions for the time-fractional TFFEM model. Li and Peng [42] applied the plane dynamical system method to derive traveling wave solutions for the equation. Wang *et al.* [43] entailed the implementation of an advanced auxiliary equation method, which culminated in the identification of the following wave solitons: dark, bright, periodic, and solitary. Akbar *et al.* [44] investigated solitary wave solutions of

the fractional-order model of the thin-film ferroelectric material equation by employing an enhanced F-expansion method.

The present study will principally examine the following form of the time-fractional TFFEM model [44] and endeavor to obtain its exact solution through the modified extended tanh function approach. The objective of this study is to provide novel contributions to the advancement of TFFEM:

$$\frac{m_d}{T_d^2}\mathrm{D}_{tt}^{\beta\beta}S-\left[\left(q_2-2\mu\right)S+q_4S^3+q_6S^5\right]-J\Delta S=0 \tag{1}$$

were $S = (x, t)$ is the unknown function, $\beta = (0, 1)$ – the fractional-order derivative, parameter m_d – the mass of ferroelectric particles, and T_d – corresponds to their charge density. The parameters q_2, q_4, and q_6 quantify temperature and pressure fields, μ is the electric susceptibility, and J governs the space inhomogeneity coefficient.

Outline of the analytical technique

Analyzing the fractional dynamical system described by:

$$P\left(f,\mathrm{D}_t^\alpha f,\mathrm{D}_x^\beta f,\mathrm{D}_t^\alpha\mathrm{D}_t^\alpha f,\mathrm{D}_t^\alpha\mathrm{D}_x^\beta f,\mathrm{D}_x^\beta\mathrm{D}_x^\beta f,\ldots\right)=0,\quad\left(0<\alpha,\beta<1\right) \tag{2}$$

were the operations $\mathrm{D}_t^\alpha f,\mathrm{D}_x^\beta f,\mathrm{D}_t^\alpha\mathrm{D}_t^\alpha f,\mathrm{D}_t^\alpha\mathrm{D}_x^\beta f,\mathrm{D}_x^\beta\mathrm{D}_x^\beta f$, *etc.*, represent fractional derivative notations. The polynomial P is analytically constructed by algebraically combining the variable u with its associated partial derivatives. In the present paper, our mathematical framework adopts the modified Riemann-Liouville fractional calculus [45] for operator definitions. The properties of this derivative are outlined in [46], as summarized:

$$\mathrm{D}_t^\alpha t^r=\frac{\Gamma\left(1+r\right)}{\Gamma\left(1+r-\alpha\right)}t^{r-\alpha} \tag{3}$$

$$\mathrm{D}_t^\alpha\left[cf\left(x\right)\right]=c\mathrm{D}_t^\alpha f\left(x\right),\quad\text{where } c\text{ is a constant} \tag{4}$$

$$\mathrm{D}_t^\alpha\left[f\left(\omega\right)+g\left(\omega\right)\right]=\mathrm{D}_t^\alpha f\left(\omega\right)+\mathrm{D}_t^\alpha g\left(\omega\right) \tag{5}$$

To address fractional-order differentiation, we apply the modified chain rule formalism as proposed in [47]:

$$\begin{gathered}\mathrm{D}_t^\alpha u=\sigma_t\frac{\partial u\left(\xi\right)}{\mathrm{d}\xi}\mathrm{D}_t^\alpha\xi,\quad\mathrm{D}_x^\alpha u=\sigma_x\frac{\partial u\left(\xi\right)}{\mathrm{d}\xi}\mathrm{D}_x^\alpha\xi\\ \mathrm{D}_t^{2\alpha}u=\left(\sigma_t\right)^2\frac{\partial^2u\left(\xi\right)}{\mathrm{d}\xi^2}\mathrm{D}_t^{2\alpha}\xi,\quad\mathrm{D}_x^{2\alpha}u=\left(\sigma_x\right)^2\frac{\partial^2u\left(\xi\right)}{\mathrm{d}\xi^2}\mathrm{D}_x^{2\alpha}\xi\end{gathered} \tag{6}$$

where σ_t and σ_x represent the sigma indices. For simplicity and without compromising generality, we set $\sigma_t = \sigma_t = L$, where L is a constant.

Step 1. Applying the fractional complex transform [47, 48]:

$$u\left(x,t\right)=u\left(\xi\right),\quad\xi=\frac{lx^\beta}{\Gamma\left(\beta+1\right)}+\frac{kt^\alpha}{\Gamma\left(\alpha+1\right)} \tag{7}$$

where l and k are non-zero constants. The fractional complex transform can be geometrically explained by the two-scale fractal geometry [49-51].

Inserting eqs. (6) and (7) into eq. (2), yields:

$$Q\left(u,u',u''\ldots\right)=0 \tag{8}$$

where $u' = \mathrm{d}u/\mathrm{d}\xi$, $u'' = \mathrm{d}^2u/\mathrm{d}\xi^2$, and Q denotes a non-linear operator encompassing u and its successive ξ-derivates.

Step 2. Supposing the ordinary differential eq. (8) has a solution in the form of a Ψ polynomial:

$$u\left(\xi\right)=\sum_{i=0}^{n}a_i\Psi^i\left(\xi\right) \tag{9}$$

where $\Psi = \Psi(\xi)$ adheres to the Riccati equation in the following form:

$$\Psi' = \varpi + \Psi^2 \tag{10}$$

where ϖ serves as a free parameter, while a_i (i = 0, 1, 2,…, n) are undetermined constants. The positive integer n is determined by balancing the orders of the highest derivative term and the highest non-linear term. For Ψ, three distinct solution classes are determined based on the different values of the constant ϖ:

$$\begin{gathered}\Psi=-\left(-\varpi\right)^{1/2}\tanh\left(-\varpi\right)^{1/2}\xi,\quad \varpi<0,\quad \Psi=-\left(-\varpi\right)^{1/2}\coth\left(-\varpi\right)^{1/2}\xi,\quad \varpi<0\\ \Psi=\left(\varpi\right)^{1/2}\tan\left(\varpi\right)^{1/2}\xi,\quad \varpi>0,\quad \Psi=\left(\varpi\right)^{1/2}\cot\left(\varpi\right)^{1/2}\xi,\quad \varpi>0\\ \Psi=\frac{-1}{\xi},\quad \varpi=0\end{gathered} \tag{11}$$

Step 3. Incorporating eq. (9) into eq. (8) and applying an iterative process with eq. (10), we group the terms of Ψ with identical powers. Subsequently, setting each coefficient term and constant item across all powers to zero. This procedure results in a system of overdetermined algebraic equations involving the parameters l, k, L, ϖ, and a_i (i = 0, 1, 2,…, n). Finally, by calculating these parameters and substituting them back into eq. (9), we derive multiple distinct types of exact solutions for eq. (2).

Novel analytical solutions of the time-fractional TFFEM model

By introducing the subsequent fractional complex transform [48]:

$$S\left(x,t\right)=S\left(\theta\right),\quad \theta=lx+\frac{kt^{\beta}}{\Gamma\left(\beta+1\right)} \tag{12}$$

the initial eq. (1) reduces to a non-linear ODE:

$$\left(\frac{m_d}{T_d^2}k^2L^2-Jl^2\right)S''-\left(q_2-2\mu\right)S-q_4S^3-q_6S^5=0 \tag{13}$$

Balancing the non-linear term, S'', with the highest order derivative term, S^5, we get $n = 1/2$. However, in accordance with the balance principle, the resulting value must be an integer that is positive. Therefore, we move on to the following transformation:

$$S(\theta) = [S(\theta)]^{1/2} \tag{14}$$

Utilizing the transformation in eq. (14) to eq. (13) results in the following form:

$$\left(\frac{m_d}{T_d^2}k^2L^2 - Jl^2\right)\left[\frac{1}{2}ss'' - \frac{1}{4}(s')^2\right] - (q_2 - 2\mu)s^2 - q_4 s^3 - q_6 s^4 = 0 \tag{15}$$

Reapplying the homogeneous balance principle to eq. (15), yielding $N = 1$.

Based on the underlying premise of the proposed method, the tentative solution for eq. (9) can be stated:

$$S(\theta) = a_0 + a_1\Psi(\theta) \tag{16}$$

Substituting eqs. (10) and (16) into eq. (15) and grouping the terms with identical powers of Ψ, and then following the coefficient elimination condition yields a non-linear algebraic overdetermined system surrounding $a_0, a_1, m_d, T_d, \mu, q_2, q_4, q_6, J, l, k, L, \varpi$:

$$\begin{gathered}
-4{a_0}^4T_d^2q_6 - 4{a_0}^3T_d^2q_4 + 4{a_0}^2T_d^2(2\mu - q_2) + {a_1}^2\left(-m_dk^2L^2 + T_d^2l^2J\right)\varpi^2 = 0 \\
4{a_0}^2T_d^2q_6 + 3a_0T_d^2q_4 - m_dk^2L^2\varpi + T_d^2\left(-4\mu + 2q_2 + l^2J\varpi\right) = 0 \\
12{a_0}^2T_d^2q_6 + 6a_0T_d^2q_4 - m_dk^2L^2\varpi + T_d^2\left(-4\mu + 2q_2 + l^2J\varpi\right) = 0 \\
{a_1}^3T_d^2q_6 + a_0a_1\left(4{a_1}^2T_d^2q_6 - m_dk^2L^2 + T_d^2l^2J\right) = 0 \\
-4{a_1}^2T_d^2q_6 + 3m_dk^2L^2 - 3T_d^2l^2J = 0
\end{gathered} \tag{17}$$

Solving this set of equations, yields several solutions for eq. (15):

Case 1.

$$\begin{gathered}
a_0 = -\frac{(3)^{1/2}(q_2 - 2\mu)^{1/2}}{2(q_6)^{1/2}}, \quad a_1 = \pm\frac{(3)^{1/2}\left(m_dk^2L^2 - T_d^2l^2J^2\right)^{1/2}}{2T_d^2(q_6)^{1/2}} \\
q_4 = \frac{4(q_6)^{1/2}(q_2 - 2\mu)^{1/2}}{(3)^{1/2}}, \quad \varpi = -\frac{T_d^2(2\mu - q_2)}{T_d^2l^2J^2 - m_dk^2L^2}
\end{gathered} \tag{18}$$

Based on the previous solution, for the original equation to have a valid real-number solution, certain conditions must be met: $m_dk^2L^2 > T_d^2l^2J^2$, $q_2 \geq 2\mu$, and $l, k \neq 0$. Therefore, in *Case 1*, considering the different values of ϖ, we find:

– When $q_2 = 2\mu$, $\varpi = 0$, which produces:

$$s_{1,2}(\theta) = \pm\frac{(3)^{1/2}\left(m_dk^2L^2 - T_d^2l^2J^2\right)^{1/2}}{2T_d^2(q_6)^{1/2}}\frac{1}{\theta}, \quad \varpi = 0 \tag{19}$$

where

$$\theta = lx + \frac{kt^{\beta}}{\Gamma(\beta+1)} \quad l,k \text{ are arbitrary constants and } l,\ k \neq 0.$$

Admitting transformation eq. (14) and the fractional wave transformation, we attain:

$$S_{1,2}(\theta) = \left[\pm \frac{(3)^{1/2}\left(m_d k^2 L^2 - T_d^2 l^2 J^2\right)^{1/2}}{2T_d^2 (q_6)^{1/2}} \frac{1}{\theta} \right]^{1/2}, \quad \varpi = 0 \tag{20}$$

The 3-D plots of $S_{1,2}(\theta)$ is shown in fig. 1.

– When $q_2 > 2\mu$, $\varpi < 0$, which produces:

$$s_{3,4}(\theta) = -\frac{(3)^{1/2}(q_2 - 2\mu)^{1/2}}{2(q_6)^{1/2}} \pm \frac{(3)^{1/2}(q_2 - 2\mu)^{1/2}}{T_d (q_6)^{1/2}} \tanh\left[\frac{T_d^2 (q_2 - 2\mu)}{m_d k^2 L^2 - T_d^2 l^2 J^2} \right]^{1/2} \theta \tag{21}$$

$$s_{5,6}(\theta) = -\frac{(3)^{1/2}(q_2 - 2\mu)^{1/2}}{2(q_6)^{1/2}} \pm \frac{(3)^{1/2}(q_2 - 2\mu)^{1/2}}{T_d (q_6)^{1/2}} \coth\left[\frac{T_d^2 (q_2 - 2\mu)}{m_d k^2 L^2 - T_d^2 l^2 J^2} \right]^{1/2} \theta \tag{22}$$

where

$$\theta = lx + \frac{kt^{\beta}}{\Gamma(\beta+1)} \quad l,k \text{ are arbitrary constants and } l,\ k \neq 0.$$

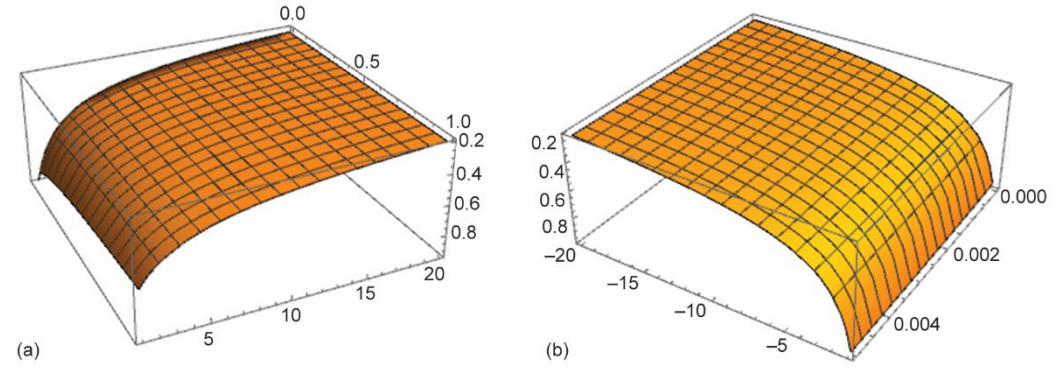

Figure 1. The 3-D plots of $S_{1,2}(\theta)$ in *Case 1* for $\beta = 1/2$, $T_d = q_6 = 2$, $m_d = k = L = J = q_2 = \mu = 1$; (a) $S_1(\theta)$ and (b) $S_2(\theta)$

According to eq. (14), yields:

$$S_{3,4}(\theta) = \left\{ -\frac{(3)^{1/2}(q_2 - 2\mu)^{1/2}}{2(q_6)^{1/2}} \pm \frac{(3)^{1/2}(q_2 - 2\mu)^{1/2}}{T_d (q_6)^{1/2}} \tanh\left[\frac{T_d^2 (q_2 - 2\mu)}{m_d k^2 L^2 - T_d^2 l^2 J^2} \right]^{1/2} \theta \right\}^{1/2} \tag{23}$$

$$S_{5,6}(\theta) = \left\{ -\frac{(3)^{1/2}(q_2 - 2\mu)^{1/2}}{2(q_6)^{1/2}} \pm \frac{(3)^{1/2}(q_2 - 2\mu)^{1/2}}{T_d (q_6)^{1/2}} \coth\left[\frac{T_d^2 (q_2 - 2\mu)}{m_d k^2 L^2 - T_d^2 l^2 J^2} \right]^{1/2} \theta \right\}^{1/2} \tag{24}$$

Since $S_{3,4}(\theta) < 0$, there are no real solutions for $S_{3,4}(\theta)$. Therefore, the graphical representations of $S_5(\theta)$ and $S_6(\theta)$ are depicted in fig. 2.

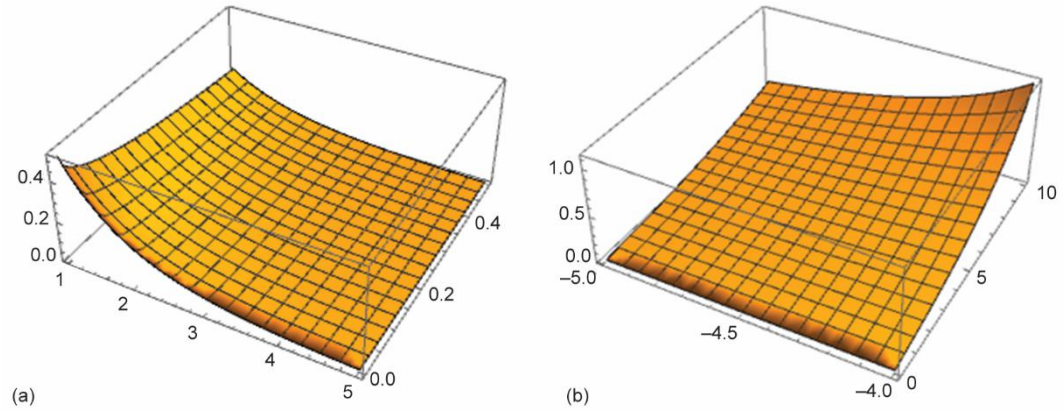

Figure 2. The 3-D plots of $S_{5,6}(\theta)$ in *Case 1* for $\beta = 1/2$, $T_d = 2$, $q_6 = 3$, $m_d = k = L = J = q_2 = \mu = 1$; (a) $S_5(\theta)$ and (b) $S_6(\theta)$

Case 2.

$$a_0 = \frac{(3)^{1/2}(q_2 - 2\mu)^{1/2}}{2(q_6)^{1/2}}, \quad a_1 = \pm\frac{(3)^{1/2}(m_d k^2 L^2 - T_d^2 l^2 J^2)^{1/2}}{2T_d^2 (q_6)^{1/2}}$$
$$q_4 = -\frac{4(q_6)^{1/2}(q_2 - 2\mu)^{1/2}}{(3)^{1/2}}, \quad \varpi = -\frac{T_d^2(2\mu - q_2)}{T_d^2 l^2 J^2 - m_d k^2 L^2} \tag{25}$$

Similarly, there must be $m_d k^2 L^2 > T_d^2 l^2 J^2, q_2 \geq 2\mu,$ and $l,\ k \neq 0$. Thus, in *Case 2*, the different values of ϖ lead to:

– When $q_2 = 2\mu$, $\varpi = 0$, and $a_0 = q_4 = 0$. The obtained solutions are the same as $S_{1,2}(\theta)$.
– When $q_2 > 2\mu$, $\varpi < 0$, which produces:

$$s_{7,8}(\theta) = \frac{(3)^{1/2}(q_2 - 2\mu)^{1/2}}{2(q_6)^{1/2}} \pm \frac{(3)^{1/2}(q_2 - 2\mu)^{1/2}}{T_d (q_6)^{1/2}} \tanh\left[\frac{T_d^2(q_2 - 2\mu)}{m_d k^2 L^2 - T_d^2 l^2 J^2}\right]^{1/2} \theta \tag{26}$$

$$s_{9,10}(\theta) = \frac{(3)^{1/2}(q_2 - 2\mu)^{1/2}}{2(q_6)^{1/2}} \pm \frac{(3)^{1/2}(q_2 - 2\mu)^{1/2}}{T_d (q_6)^{1/2}} \coth\left[\frac{T_d^2(q_2 - 2\mu)}{m_d k^2 L^2 - T_d^2 l^2 J^2}\right]^{1/2} \theta \tag{27}$$

where

$$\theta = lx + \frac{kt^{\beta}}{\Gamma(\beta + 1)}$$

l, k are arbitrary constants and $l,\ k \neq 0$.

Based on eq. (14), the following results are derived:

$$S_{7,8}(\theta)=\left\{\frac{(3)^{1/2}(q_2-2\mu)^{1/2}}{2(q_6)^{1/2}}\pm\frac{(3)^{1/2}(q_2-2\mu)^{1/2}}{T_d(q_6)^{1/2}}\tanh\left[\frac{T_d^2(q_2-2\mu)}{m_dk^2L^2-T_d^2l^2J^2}\right]^{1/2}\theta\right\}^{1/2} \quad (28)$$

$$S_{9,10}(\theta)=\left\{\frac{(3)^{1/2}(q_2-2\mu)^{1/2}}{2(q_6)^{1/2}}\pm\frac{(3)^{1/2}(q_2-2\mu)^{1/2}}{T_d(q_6)^{1/2}}\coth\left[\frac{T_d^2(q_2-2\mu)}{m_dk^2L^2-T_d^2l^2J^2}\right]^{1/2}\theta\right\}^{1/2} \quad (29)$$

The numerical simulation images of $S_7(\theta)$, $S_8(\theta)$, $S_9(\theta)$, and $S_{10}(\theta)$ are shown in fig. 3.

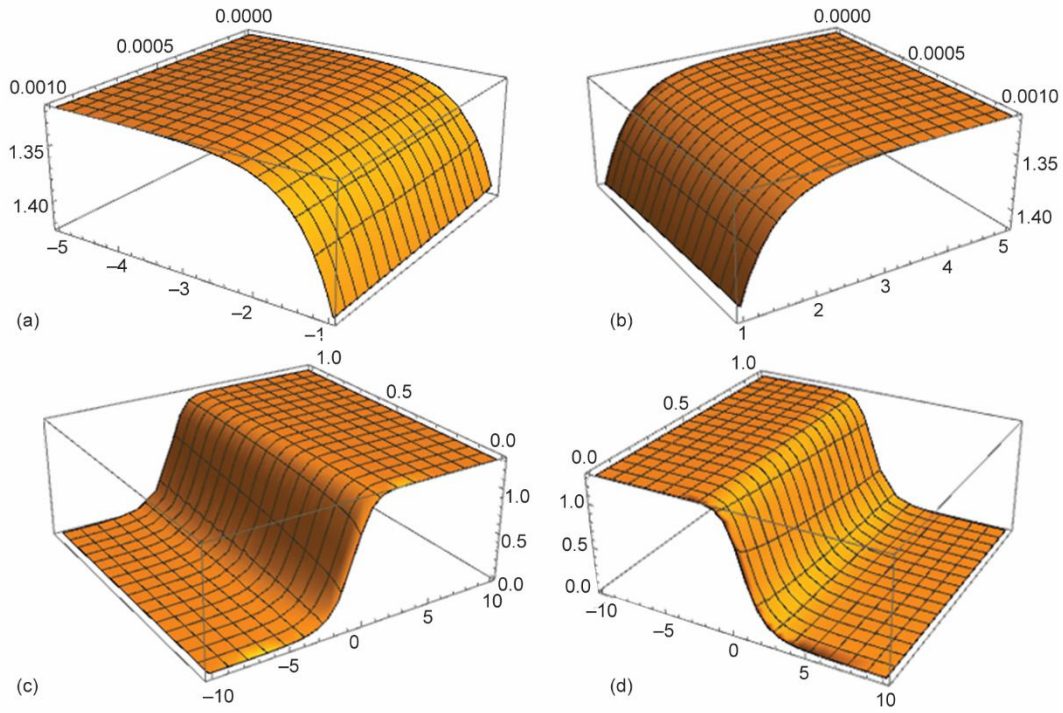

Figure 3. The 3-D plots of $S_{7,8}(\theta)$ and $S_{9,10}(\theta)$ in *Case 2* for $\beta = 1/2$, $T_d = 2$, $q_6 = 3$, $m_d = k = L = J = q_2 = \mu = 1$; (a) $S_7(\theta)$, (b) $S_8(\theta)$, (c) $S_9(\theta)$, and (d) $S_{10}(\theta)$

Conclusion

The present study focuses on the time-fractional TFFEM model and employs the modified extended tanh-function approach to derive eight new exact solutions for this significant material model, in addition to visualizations of these solutions. These innovative analytical solutions offer novel insights into understanding the non-linear behavior of TFFEM under varying pressures, temperatures, and other parameter values, and may contribute to the advancement of TFFEM.

Acknowledgment

This research was funded by the Summit Advancement Disciplines of Zhejiang Province (Zhejiang Gongshang University - Statistics), "Digital+" Discipline Construction Management Project of Zhejiang Gongshang University (SZJ2022B004) , Collaborative Innovation Center of Statistical Data Engineering Technology & Application and the phased achievements of the provincial first-class course "Market Survey and Forecasting" in Hunan Province.

References

[1] Mathew, S., *et al.* Dispersion Characteristics of Superconducting Coplanar Waveguide Structure Based on Ferroelectric Thin Film, *J Supercond Nov Magn, 38* (2025), 90
[2] Wu, J., *et al.*, High Electron Mobility and Quantum Oscillations in Non-Encapsulated Ultrathin Semiconducting Bi_2O_2Se, *Nature Nanotech*, *12* (2017), 6, pp. 530-534
[3] Chen, C., *et al.*, Growth of Single-Crystal Black Phosphorus and its Alloy Films through Sustained Feedstock Release, *Nature Materials, 22* (2023), 6, pp. 717-724
[4] He, J.-H., *et al.*, Modeling and Numerical Analysis for an MEMS Graphene Resonator, *Front. Phys. 13* (2025), 1551969
[5] He, J.-H., Periodic Solution of a Micro-Electromechanical System, *Facta Universitatis, Series: Mechanical Engineering, 22* (2024) , 2, pp. 187-198
[6] Cao, R., *et al.*, Softening of the Optical Phonon by Reduced Interatomic Bonding Strength without Depolarization, *Nature*, *634* (2024), Oct., pp. 1080-1085
[7] Setter, N., *et al.*, Ferroelectric Thin Films: Review of Materials, Properties, and Applications, *Journal of Applied Physics, 100* (2006), 051606
[8] Lane, W. M., Rappe, A. M., Thin-Film Ferroelectric Materials and Their Applications, *Nature Reviews Materials, 2* (2017), 16087
[9] Cheema, S. S., *et al.*, Enhanced Ferroelectricity in Ultrathin Films Grown Directly on Silicon, *Nature, 580* (2020), Apr., pp. 478-482
[10] Wang, Y., *et al.*, Ultrathin Ferroelectric Films: Growth, Characterization, Physics and Applications, *Materials*, *7* (2014), 9, pp. 6377-6485
[11] Cui, B., *et al.*, Ferroelectric Photosensor Network: An Advanced Hardware Solution to Real-Time Machine Vision, *Nature Communications*, *13* (2022), 1707
[12] Guo, J., *et al.*, A Freestanding Ferroelectric Thin Film-Based Soft Strain Sensor, *Journal of Materiomics, 11* (2025), 100830
[13] Petritz, A., *et al.*, Imperceptible Energy Harvesting Device and Biomedical Sensor Based on Ultraflexible Ferroelectric Transducers and Organic Diodes, *Nature Communications*, *12* (2021), 2399
[14] He, J.-H. , *et al.*, Piezoelectric Biosensor Based on Ultrasensitive MEMS System, *Sensors and Actuators A: Physical*, *376* (2024), 115664
[15] Qian, M. Y., *et al.*, Enhanced Piezoelectric Performance of PVDF Nanofibers by Biomimicking the Spider's Long Liquid Transport, *Chemical Engineering Journal*, *483* (2024), 149159
[16] Zhang, H. Y., *et al.*, Biodegradable Ferroelectric Molecular Crystal with Large Piezoelectric Response, *Nature Nanotech*, *12* (2017), 6, pp. 530-534
[17] Park, J., *et al.*, Fingertip Skin-Inspired Microstructured Ferroelectric Skins Discriminate Static/Dynamic Pressure and Temperature Stimuli, *Science Advances, 1* (2015), 1500661
[18] Polla, D. L., Francis, L.F., Ferroelectric Thin Films in Micro-Electromechanical Systems Applications, *MRS Bulletin, 21* (1996), 21, pp. 59-65
[19] Dong, G., *et al.*, Super-Elastic Ferroelectric Single-Crystal Membrane with Continuous Electric Dipole Rotation, *Science, 366* (2019), 6464, pp. 475-479
[20] Li, S., *et al.*, Ferroelectric Thin Films: Performance Modulation and Application, *Materials Advances, 3* (2022), 14, pp. 5735-5752
[21] Shao, M. H., *et al.*, Challenges and Recent Advances in HfO_2-Based Ferroelectric Films for Non-Volatile Memory Applications, *Chip, 3* (2024), 100101
[22] Liao, J., *et al.*, HfO_2-Based Ferroelectric Thin Film and Memory Device Applications in the Post-Moore Era: A Review, *Fundamental Research, 3* (2023), 3, pp. 332-345

[23] Pan, Z., *et al.*, Substantially Improved Energy Storage Capability of Ferroelectric Thin Films for Application in High-Temperature Capacitors, *Journal of Materials Chemistry A, 14* (2021), 9, pp. 9281-9290
[24] Pond, J., *et al.*, Microwave Properties of Ferroelectric Thin Films, *Integrated Ferroelectrics, 22* (1998), 4, pp. 317-328
[25] Su, H. T., *et al.*, Electrically Tunable Superconducting Quasilumped Element Resonator Using Thin-Film Ferroelectrics, *Microwave and Optical Technology Letters, 24* (2000), 3, pp. 155-158
[26] Liu, C., *et al.*, Low Voltage-Driven High-Performance Thermal Switching in Antiferroelectric $PbZrO_3$ Thin Films, *Science, 382* (2023), 6676, pp. 1265-1269
[27] Zhang, G., *et al.*, Thin Film Ferroelectric Photonic-Electronic Memory, *Light: Science & Applications, 13* (2024), 206
[28] Gupta, R., *et al.*, High Frequency Coplanar Microwave Resonator Using Ferroelectric Thin Film for Wireless Communication Applications, *Materials Today: Proceedings, 5* (2018), 7, pp. 15395-15398
[29] Li, S., *et al.*, Ferroelectric Thin Films: Performance Modulation and Application, *Materials Advances, 3* (2022), 14, pp. 5735-5752
[30] Ali, F., *et al.*, Fluorite-Structured Ferroelectric and Antiferroelectric Materials: A Gateway of Miniaturized Electronic Devices, *Advanced Functional Materials, 32* (2022), 2201737
[31] Hubert, M. B., *et al.*, Solitons in Thin-Film Ferroelectric Material, *Physica Scripta, 93* (2018), 075201
[32] Zahran, E. H., *et al.*, Study on Abundant Explicit Wave Solutions of the Thin-Film Ferro-Electric Materials Equation, *Optical and Quantum Electronics, 54* (2022), 48
[33] Bekir, A., Zahran, E. H. M., Optical Soliton Solutions of the Thin-Film Ferro-Electric Materials Equation According to the Painleve Approach, *Optical and Quantum Electronics, 53* (2018), 118
[34] Bekir, A., *et al.*, New Optical Soliton Solutions for the Thin-Film Ferroelectric Materials Equation Instead of the Numerical Solution, *Computational Methods for Differential Equations, 10* (2022), 1, pp. 158-167
[35] Chu, Y. M., *et al.*, Solitary Wave Dynamics of Thin-Film Ferroelectric Material Equation, *Results in Physics, 45* (2023), 106201
[36] Souleymanou, A., *et al.*, The Propagation of Waves in Thin-Film Ferroelectric Materials, *Pramana, 93* (2019), 27
[37] Chen, D., Li, Z., New Optical Soliton Solutions of Thin-Film Ferroelectric Material Equation via the Complete Discrimination System Method, *Results in Physics, 50* (2023), 106551
[38] Sadaf, M., *et al.*, Soliton Solutions of Thin-Film Ferroelectric Materials Equation, *Results in Physics, 58* (2024), 107380
[39] Rahman, R. U., *et al.*, Dynamical Behavior of Fractional Non-Linear Dispersive Equation in Murnaghan's Rod Materials, *Results in Physics, 56* (2024), 107207
[40] Zeng, H. J., *et al.*, Exact Solutions of a Class of Generalized Nanofluidic Models, *Open Physics, 22* (2024), 20240068
[41] Faribi, W. A., *et al.*, Exact Fractional Soliton Solutions of Thin-Film Ferroelectric Material Equation by Analytical Approaches, *Alexandria Engineering Journal, 78* (2023), Sept., pp. 483-497
[42] Li, Z., Peng, C., Bifurcation, Phase Portrait and Traveling Wave Solution of Time-Fractional Thin-Film Ferroelectric Material Equation with Beta Fractional Derivative, *Physics Letters A, 484* (2023), 129080
[43] Wang, X., *et al.*, Analytical Solitary Wave Solutions of a Time-Fractional Thin-Film Ferroelectric Material Equation Involving Beta-Derivative Using Modified Auxiliary Equation Method, *Results in Physics, 48* (2023), 106411
[44] Akbar, M. A., *et al.*, Mathematical Analysis of the Dynamics of Solitary Wave Solutions to the Time-Fractional Thin-Film Ferroelectric Materials Model, *Results in Physics, 60* (2024), 107621
[45] Jumarie, G., Modified Riemann-Liouville Derivative and Fractional Taylor Series of Nondifferentiable Functions Further Results, *Computers and Mathematics with Applications, 51* (2006), 9-10, pp. 1367-1376
[46] Jumarie, G., Fractional Partial Differential Equations and Modified Riemann-Liouville Derivative New Methods for Solution, *Journal of Applied Mathematics and Computing, 24* (2007), 1-2, pp. 31-48
[47] He, J.-H., *et al.*, Geometrical Explanation of the Fractional Complex Transform and Derivative Chain Rule for Fractional Calculus, *Physics Letters A, 376* (2012), 4, pp. 257-259
[48] Li, Z. B., He, J.-H., Fractional Complex Transform for Fractional Differential Equations, *Mathematical and Computational Applications, 15* (2010), 5, pp. 970-973

[49] Zuo, Y. T., *et al.*, Gecko-Inspired Fractal Buffer for Passenger Elevator, *Facta Universitatis, Series: Mechanical Engineering*, *22* (2024), 4, pp. 633-642
[50] He, C. H., *et al.*, A Fractal-Based Approach to the Mechanical Properties of Recycled Aggregate Concretes, *Facta Universitatis, Series: Mechanical Engineering*, *22* (2024), 2, pp. 329-342
[51] Zhang, Y. R., *et al.*, Fast and Accurate Population Forecasting with Two-Scale Fractal Population Dynamics and Its Application to Population Economics, *Fractals*, *32* (2024), 2450082

Paper submitted: November 10, 2024
Paper revised: May 12, 2025
Paper accepted: May 12, 2025
2026 Published by the Vinča Institute of Nuclear Sciences, Belgrade, Serbia.
This is an open access article distributed under the CC BY-NC-ND 4.0 terms and conditions.